Rev. Adv. Mater. Sci. 32 (2012) 34-43

THE EFFECT OF NANOSIZE Y_2O_3-ZrO_2, Ce_2O_3-ZrO_2, AND Ce_2O_3-Y_2O_3-ZrO PRECURSOR DISPERSITY ON THE CONDUCTIVITY AND SENSOR PROPERTIES OF FINAL CERAMICS

V.G. Konakov[1,2,3], A.V. Shorokhov[4], N.V. Borisova[2], S.N. Golubev[2], E.N. Solovieva[2,3] and V.M. Ushakov[2]

[1]Chemical Department, St. Petersburg State University, St. Petersburg, Russia
[2]Institute for Problems of Mechanical Engineering, St. Petersburg, Russia
[3]Science and Technical Center "Glass and Ceramics", St. Petersburg, Russia
[4]Smolensk State Production Union "Analitpribor", Smolensk, Russia

Received: January 19, 2012

Abstract. Nanosize precursors with controlled dispersity were synthesized using the reverse co-precipitation sol-gel method by varying the concentrations of the initial salt solutions. A set of final ceramics ($0.08Y_2O_3$-$0.92ZrO_2$, $0.09Ce_2O_3$-$0.91ZrO_2$, $0.06Ce_2O_3$-$0.06Y_2O_3$-$0.88ZrO_2$, mol.%) was produced from the precursor powders of different dispersity; their conductivity and sensor properties were investigated. As a result, $0.08Y_2O_3$-$0.92ZrO_2$ ceramics manufactured from the precursor powders with the average agglomerate size of 100-140 nm was shown to be the optimal choice for the use as a solid electrolyte with anionic conductivity.

1. INTRODUCTION

Solid electrolytes with ionic conductivity represent a specific group among the zirconia based materials widely used by modern industry [1-3]. Modern technologies commonly apply fluorite type zirconia solid solutions stabilized by CaO, MgO, Y_2O_3 or rare-earth oxide additions. Rather high unipolar ionic conductivity of such solid solutions at high temperatures gives an opportunity to use them in different applications: as solid electrolytes in galvanic elements in fuel cells; oxygen sensors for the determinations of the completeness of fuel burning in the internal combustion engines and other power machines, in ferrous and non-ferrous metallurgy, glass and refractory production, etc.; the basic task here is the oxygen partial pressure monitoring. Since the required conductivity level in these materials is usually achieved at rather high temperatures, modern science continues the development of new materials providing the possibility to increase the temperature range of sensor applicability and to improve their sensitivity to oxygen partial pressures.

Basing on the modern literature data, $0.08Y_2O_3$-$0.92ZrO_2$, $0.09Ce_2O_3$-$0.91ZrO_2$, $0.06Ce_2O_3$-$0.06Y_2O_3$-$0.88ZrO_2$ (mol.%) were chosen as the perspective compositions for such materials and sol-gel synthesis – as an optimal production method [4]. The idea of this method is the manufacturing of zirconia and doping cations hydroxide gels using various approaches; these gels are then dried at 373-473K, as a result, so-called precursor powders (precursors) are produced. These precursor powders are then exposed to intermediate heat treatment, compacting, and final heat treatment at 1773-1973K. The advantage of this approach is the possibility of the production of nanostructures solid electrolytes

Corresponding author: V.G. Konakov, e-mail: glasscer@yandex.ru

with improved physical and chemical properties (chemical and thermal stability, mechanical strength, vacuum density, etc.).In addition, it is believed that these materials will possess high ionic conductivity in wider temperature and oxygen partial pressure ranges in comparison with the conventional ceramics manufactured by solid-phase synthesis or by some other traditional industrial approaches.

The aims of the present work were:

(1) synthesis of the nanosized precursor powders of the above mentioned compositions with controlled dispersity using sol-gel method and the production of nanostructured solid electrolytes on their base.

(2) the study of the effect of the particle size in the precursor powders on the conductivity and sensor properties of the final ceramics.

2. EXPERIMENTAL

$0.08Y_2O_3$-$0.92ZrO_2$, $0.09Ce_2O_3$-$0.91ZrO_2$, $0.06Y_2O_3$-$0.06Ce_2O_3$-ZrO_2 gels and precursor powders were synthesized using the reverse co-precipitation sol-gel method. The initial reagents were: $Y(NO_3)_3{\cdot}6H_2O$, $ZrO(NO_3)_2{\cdot}2H_2O$, $Ce(NO_3)_3{\cdot}6H_2O$ and ammonia aqueous solution. At the first step, the aqueous solutions of the above listed salts were prepared, they were taken in the ratio necessary for the obtaining of 0.1 mole of the final product of the chosen composition. The mixture of the aqueous solutions was thoroughly mixed. At the next step, the mixture was added by drops into the 1M ammonia aqueous solution, the addition rate was 20 mL per hour. At that, the volume of ammonia solution was 10 times higher than that of the salts mixture; this fact gives the opportunity to maintain the constant pH level of about 9-10. Co-precipitation proceeds at 273K in the ice bath at permanent mixing by multiblade mechanical agitator; as a result, the hydroxide mixture was formed. The excess of NH_4OH forming NH_4NO_3, and some part of water was removed by centrifugation. The gel was then intensively mixed for 10 minutes, after that it was filtered on the Buchner funnel through the MFFI-2G filter (composite based F-42 fluoroplastic) with the average pore size of ~ 250 nm and washed by distilled water up to the neutral reaction of the washing liquid and the absence of the characteristic reaction on NO_3^{1-} ion in it. At the following step, the washed gels were dried under pressure at 423K. To do that, we have placed the gels between two smooth and chemically inert surfaces and press them under the load of 5 kg/cm^2. The difference in the precursor powders dispersity was obtained by varying the initial salt solution concentrations.

To study the conductivity and sensor properties of the final ceramics, gels were heat treated at 823K, and the pellets of 7.2 mm in diameter and 4 mm in height were formed; these pellets were then consequentially compacted without bindings at 45 and 1500 atm. The final part of pellets preparation was 2-hours heat treatment at 1873K.

According the data reported in [5], CeO_2 and Ce_2O_3 are the most stable cerium oxides, note that the content of Ce^{4+} ion in cerium oxides increases with the temperature decrease. With regard to this fact, the CeO_2 and Ce_2O_3 ratio in precursor powders and final ceramics was controlled by X-ray photoelectron spectrometer ESCA-5400, PHI. $Mg_{K\acute{a}}$ irradiation with the energy of 1253.6 eV was used for photoelectron excitation, the energetic scale was calibrated using Au $4f_{7/2}$ line with E_b = 84.0 eV. The depth of such analyses was about 50 Å and the analyzed area ~ 1 mm in diameter. The results showed that Zr in all samples was in ZrO_2 form, cerium – in CeO_2 and Ce_2O_3 forms, and Y was basically in Y_2O_3 form with the small addition of non-stoichiometric $YO_{1.5-x}$ oxide.

Precursor powders and final ceramics samples were studied by the following approaches:

- Differential scanning calorimetry (DSC) in the regime of differential thermal analysis (calorimeter Netczh DSC 404C); temperatures and types (endo- or exo-) of phase transitions were determined;
- XRD – analysis was performed using SHIMADZU XRD-6000, Cu-K_α irradiation (1.54 Å), at 30 kV bias and 30 mA current; phase composition was established;
- Adsorption-desorption isotherms were measured using Quantachrome Nova 1200e analyzer at the temperature of liquid nitrogen (77.35K), gaseous nitrogen was applied as adsorbing agent; the relative surface area for the precursor powders was determined by BET method;
- Particle-size distribution (PSD) analysis was performed by Horiba LA-950, ultrasound was used to destroy agglomerates; the distribution of the agglomerate size in the precursor powders was detected;
- TEM analyses were done by JEOL JEM 3000F electron microscope with the accelerating voltage of 300 kV; the agglomerate size in the precursors was investigated.

The relative surface area of the agglomerates in the precursor powders within the BET method was calculated as:

$$S_{BET} = \left(W_m N A_{CS}\right)/\left(Mm\right),$$

where: W_m is the weight of the adsorbed gas that covers the complete surface of the particles in the form of monolayer; N - Avogadro's number; M – the nitrogen molecular weight; A_{CS}=16.2 Å^2 – the cross-section area for the nitrogen monolayer (at that, it is supposed that adsorbed nitrogen monolayer has the hexagonal packing. In addition, it exists in the state identical to that of nitrogen in the volume of liquid nitrogen. So, the density of this monolayer can be taken equal to the density of liquid nitrogen.

3. RESULTS AND DISCUSSION

Agglomerate size in the precursor powders

The systematic study of the effect of the salts solution concentrations on the agglomerate size in the precursor powders was carried out by BET, TEM, and PSD methods. Figs. 1 and 2 demonstrate the results of TEM analysis. As seen from the figures, the agglomerate size increases with the increase of the initial salts concentration. Fig. 1c indicates that the agglomerates are formed from the particles with the average size ≈60 nm. Table 1 summarizes the results obtained by BET, PSD, and DSC for the $0.08Y_2O_3$-$0.92ZrO_2$ precursors.

The dependence of the average agglomerate size determined by PSD analysis for the precursor powders with $0.09Ce_2O_3$-$0.91ZrO_2$ and $0.06Ce_2O_3$-$0.06Y_2O_3$-$0.88ZrO_2$ compositions on the initial salts concentration is presented in Fig. 3. As seen from the figure, the agglomerate size in the above listed precursors increases smoothly with salts concentration in the concentration range up to ≈0.5M. The following concentration increase (>0.5M) results in the rapid growth of the average agglomerate size. Possibly, it is due to the fact that a huge number of nucleation centers is formed in the solution at such concentrations, these nuclei,

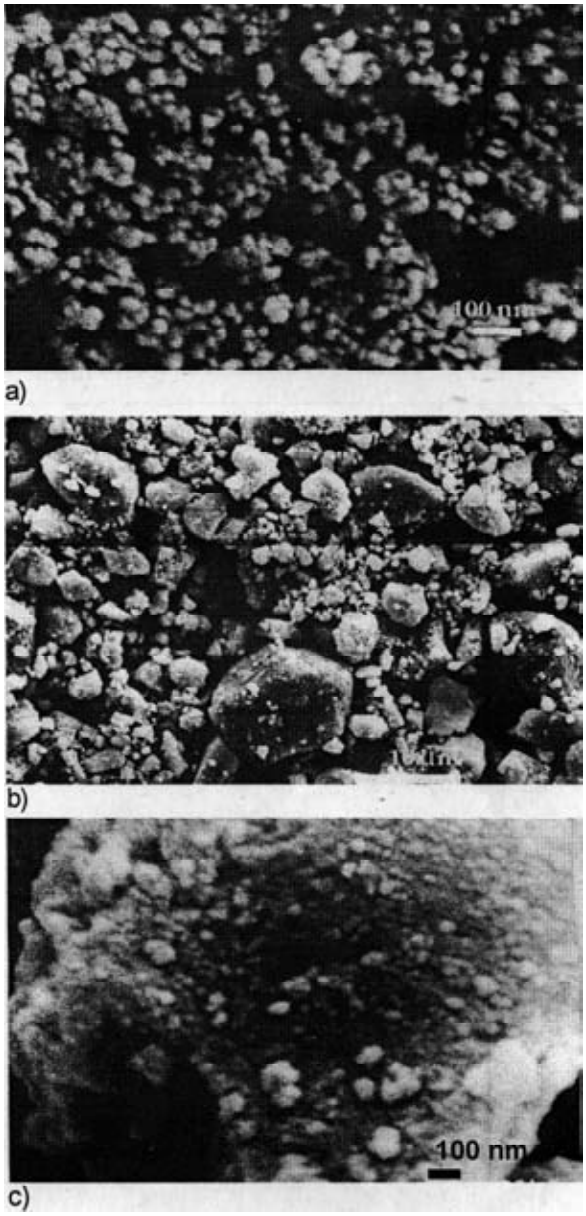

Fig. 1. Microphotographs of the precursors with the $0.08Y_2O_3$-$0.92ZrO_2$ final composition produced from the solutions with the concentrations of the initial salts of 0.01M (a), 1.2M (b), and 0.05(c) .

Table 1. The dependence of the average agglomerate size in $0.08Y_2O_3$-$0.92ZrO_2$ precursors and their crystallization temperature on the salt concentration.

Salt concentration, M	Average agglomerate size (d_{BET}), nm	Relative surface area, m^2/g	Crystallization temperature, K
0.01	42	140.15	702
0.05	58	97.4	717
0.1	96	62.1	747
0.4	510	14.0	912
0.6	815	13.8	948
0.8	2400	11.4	958
1.2	1000	-	1000

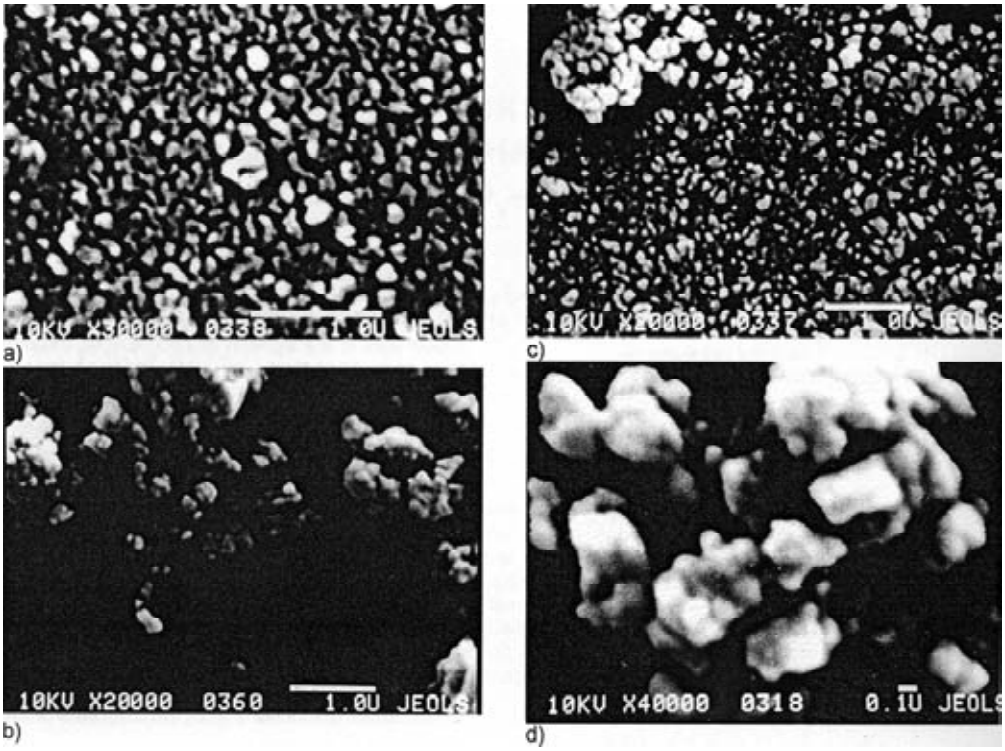

Fig. 2. Microphotographs of the precursors with the $0.09Ce_2O_3$-$0.91ZrO_2$ final composition produced from the solutions with the concentrations of the initial salts of 0.05M (a), 0.1M (b), and 0.85M (c, d).

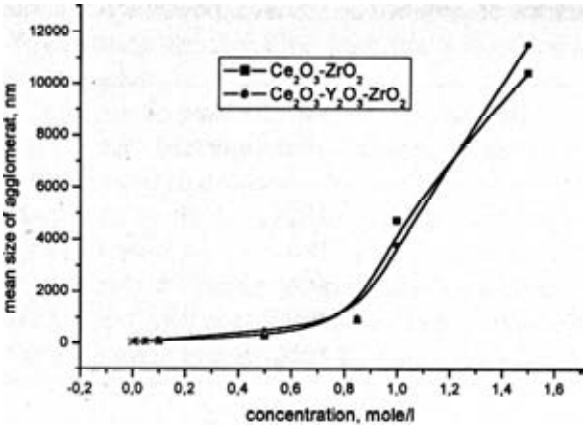

Fig. 3. The dependence of the average agglomerate size determined for the precursor powders with $0.09Ce_2O_3$-$0.91ZrO_2$ and $0.06Ce_2O_3$-$0.06Y_2O_3$-$0.88ZrO_2$ compositions on the initial salts concentration.

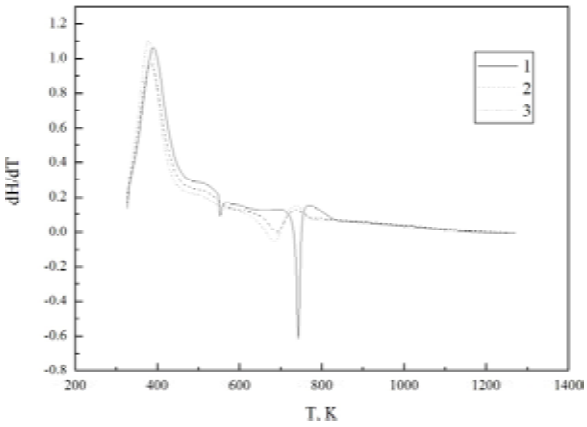

Fig. 4. DSC data for the $0.08Y_2O_3$-$0.92ZrO_2$ (1),$0.09Ce_2O_3$-$0.91ZrO_2$ (2), and $0.06Ce_2O_3$-$0.06Y_2O_3$-$0.88ZrO_2$ (3) precursors with the average agglomerate size of 100-150 nm after the 1 hour heat treatment at 473K.

enlarging in size, give rise to a rapid formation of large aggregates. Besides, the decrease in the precursor dispersity is accompanied by the increase in their crystallization temperature, see Table 1.

Thermal evolution of the precursors

The effect of heat treatment on the average agglomerate size was revealed by DSC method. Figs. 4 and 5 demonstrate the identified regularities for the precursors with the average agglomerate size of 100-150 nm treated at 473 and 1773K. Thermograms of the precursors treated at 473K indicate the presence of endothermic effects at temperature ~ 373K and exothermic effects in the temperature range 673-773K, while the thermograms of the precursors treated at 1773K proves their high crystallinity level.

According to the XRD data (Figs. 6 and 7), the precursors are basically disordered, however, the presence of low expressed peaks in 30° region (this is the typical region for the intensive reflexes for the

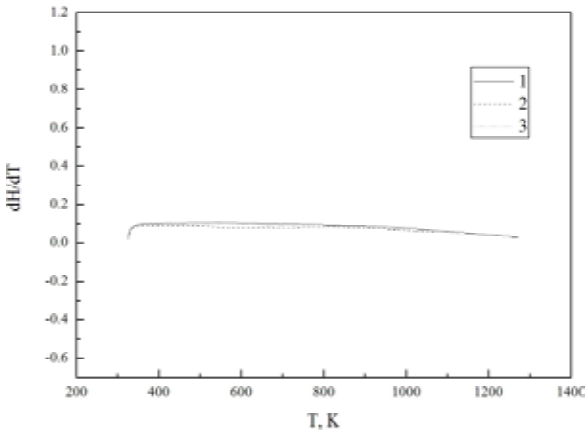

Fig. 5. DSC data for the $0.08Y_2O_3$-$0.92ZrO_2$ (1),$0.09Ce_2O_3$-$0.91ZrO_2$ (2), and $0.06Ce_2O_3$-$0.06Y_2O_3$-$0.88ZrO_2$ (3) precursors with the average agglomerate size of 100-150 nm after the 1 hour heat treatment at 1773K.

crystalline solid solutions) can be treated as the indication of the possibility of the crystalline phase presence. The crystallinity of the samples increases with the heat treatment temperature. Both after the calcination at 873K and heat treatment at 1273K, as well as after the final treatment at 1773K, the crystalline phase is cubic solid solutions for $0.08Y_2O_3$-$0.92ZrO_2$ and $0.06Ce_2O_3$-$0.06Y_2O_3$-$0.88ZrO_2$ samples and tetragonal solid solutions for $0.09Ce_2O_3$-$0.91ZrO_2$ samples, see Figs. 6 and 7 (PDF database [6] was used for the diffractograms identification).

Precursor dispersity and conductivity of solid electrolytes

One of the principal requirements applied to oxide electrolytes with anionic conductivity is the high level of such conductivity – about 10^{-1}-10^{-3} Ohm^{-1}"cm^{-1} [7]. For this reason, the study of the temperature dependencies of the conductivity of the produced electrolytes was carried out. It was performed at 1 kHz alternating current by two-electrode method in the temperature range 723-1035K using the home-made device designed at the physical chemistry laboratory of the chemical department of St. Petersburg State University. The measurement procedure was as follows. Both sides of the ceramic pellets produced by the above described approach were polished; after that they were thoroughly cleaned, and the thickness of the pellets was measured with the accuracy better than ±0,01mm. After that, the graphite electrodes were deposited on both sides of the pellets. The prepared samples were then fixed by holders with platinum contacts in the measuring cell, which, in turn, was placed

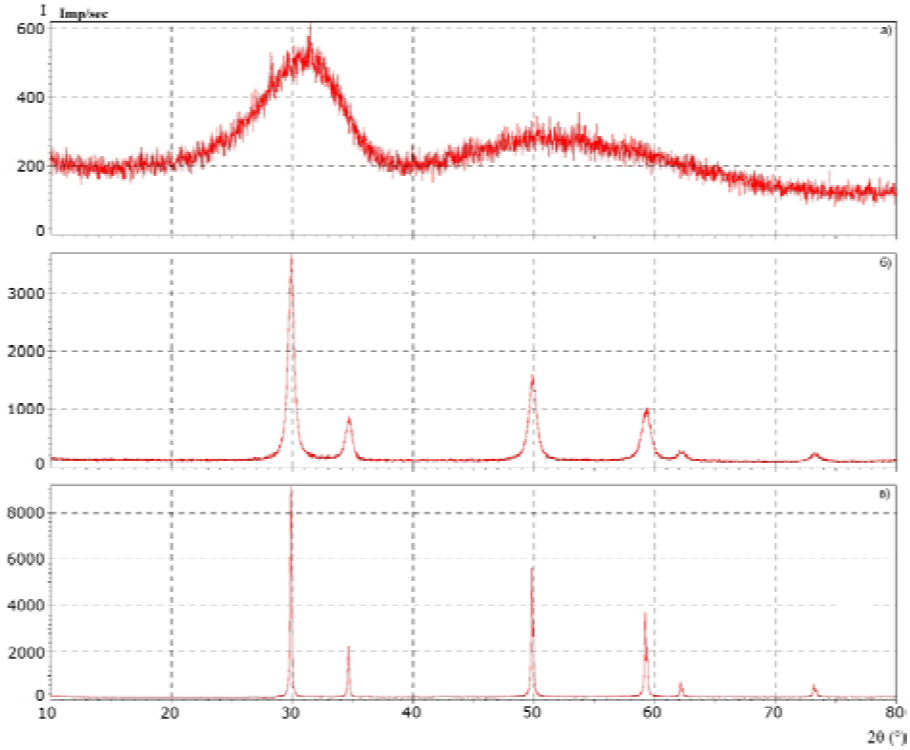

Fig. 6. XRD data for $0.06Y_2O_3$-$0.06Ce_2O_3$-$0.88ZrO_2$ sample: (a) after the drying at 423K under 5 kg/cm^2 pressure; after the heat treatment at 873K (b) and 1273K (c). The average agglomerate size in the precursor is 100-150 nm.

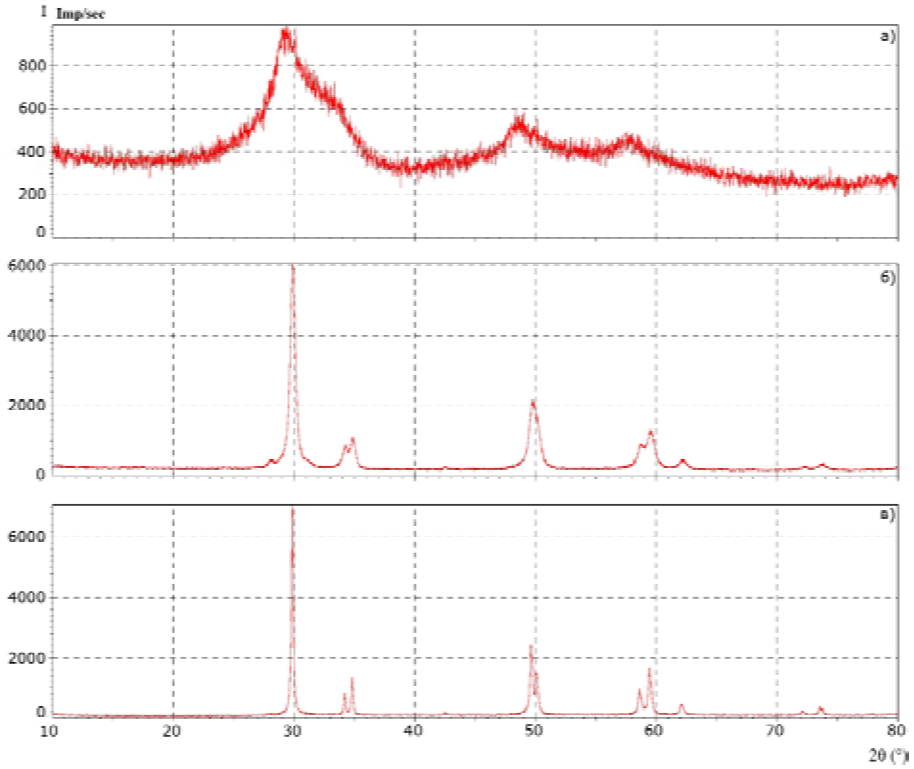

Fig. 7. XRD data for $0.09Ce_2O_3$-$0.91ZrO_2$ sample: (a) after the drying at 423K under 5 kg/cm^2 pressure; after the heat treatment at 873K (b) and 1273K (c). The average agglomerate size in the precursor is 100-150 nm.

into the furnace with regulated temperature; the accuracy of the temperature measurement was ±0.1K. The relative resistance was calculated using the formula $\rho = rS/L$, where r was the resistance of the sample, L – its thickness, and S – the area of the graphite electrode (1 cm^2). For all studied samples, the dependencies of the relative resistance (ρ) on reverse temperature (T) can be presented by linear approximation (Figs. 8 and 9); this fact gives an opportunity to use the well-known equation for the relative conductivity of the crystals (σ) [8]:

$$\sigma = \sigma_0 \exp\left(-E_a / RT\right). \quad (1)$$

Since $\sigma = 1/\rho$, Eq. (1) can be easily rewritten as:

$$\lg \rho = \lg \rho_0 + E_a / 2,303RT, \quad (2)$$

where: ρ_0 is the pre-exponential factor equal to relative resistance at $T \to \infty$, E_a – the conductivity activation energy, and R – the universal gas constant.

Fig. 8 demonstrates the decrease in the resistance of the $0.08Y_2O_3$-$0.92ZrO_2$ electrolyte: the resistivity of the sample decreases twice with the decrease in the average agglomerate size in the precursor powder from 200-250 to 40 nm. Since the decrease of the average agglomerate size in the precursor leads to the decrease of the average crystallite size which affect the formation of the crystallite agglomerates (grains) in the final ceramics, it is reasonable to suggest that the discussed resistance decrease is due to the decrease in the inputs of both surface and volume grain resistances in the total resistance. This assumption correlates with the conclusions done in [9,10]; these works also claim the decrease of the inputs of surface and volume grain resistances with the decrease in the average crystallite size. The following interesting fact should be also noted: E_a value evaluated from the tangent of the slope angles of the lines plotted in Fig. 8 is practically independent from the average agglomerate size in the precursors, it is 0.9-0.95 eV.

Fig. 9 illustrates the temperature dependencies of the resistivity of the ceramics with different compositions synthesized from the precursors with the same average size of the agglomerates. As seen from the figure, the lowest resistivity was measured for cerium-zirconia ceramics; this fact can be explained as being due to the presence of the significant amount of multivalent Ce ions in it. The estimates of E_a values for different cerium-containing ceramics lead to the same value of 0.82 eV.

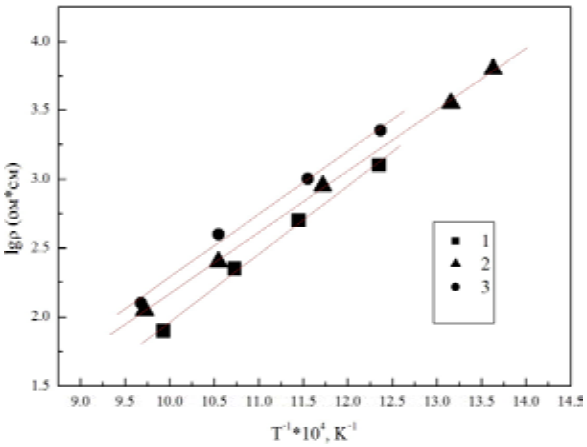

Fig. 8. Temperature dependencies of the resistivity of $0.08Y_2O_3$-$0.92ZrO_2$ solid electrolytes synthesized from the precursors with the average agglomerate sizes: 1 - 40, 2 - 120÷140, and 3 - 200÷250 nm.

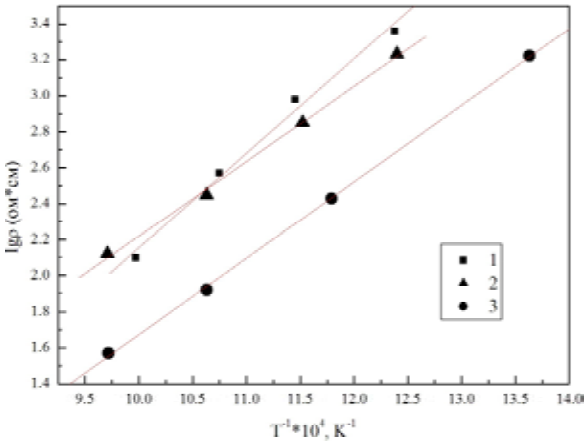

Fig. 9. Temperature dependencies of the resistivity of $0.08Y_2O_3$-$0.92ZrO_2$ (1), $0.06Ce_2O_3$-$0.06Y_2O_3$-$0.88ZrO_2$ (2) and $0.09Ce_2O_3$-$0.91ZrO_2$ (3) solid electrolytes synthesized from the precursors with the average agglomerate size of 100÷140 nm.

Thus, the results presented in this section prove that the studied ceramics produced from the precursor powders with the average agglomerate size in the range 40-250 nm could be recommended for the practical use as solid electrolytes in the temperature range 730-1000K.

Precursor dispersity and sensor properties of solid electrolytes

It is well known that fluorite-like oxide solid electrolytes based on zirconia are used as solid electrolytes in the galvanic element O_2 ($P_{O2}^{(1)}$), Pt | ТЭ | Pt, ($P_{O2}^{(2)}$), which, in turn, is conventionally used in oxygen sensors. Since such solid electrolytes are electron-ion conductors in the wide range of temperatures and oxygen pressures, the measured electromotive force of the galvanic element (E_{real}) is equal to [11]

$$E_{real} = \frac{2,303RT}{4F} \cdot t_{ion} \cdot \lg \frac{P_{O2}^{(1)}}{P_{O2}^{(2)}}, \qquad (3)$$

where R is the universal gas constant, T – absolute temperature, F – Faraday's number, $t_{ion.}$ – the transport number for oxygen ions, and $P_{O2}^{(1)}$ and $P_{O2}^{(2)}$ – oxygen partial pressures in the semicells of the galvanic element.

At $t_{ion} = 1$, Eq. (3) is the well-known Nernst equation (E_{Nernst}), and t_{ion} for the studied electrolyte will be equal to E_{real}/E_{Nernst}.

Fig. 10 demonstrates the scheme of the sensor construction which was developed for the investigation of the sensor properties of the oxygen sensors based on the studied solid electrolytes. $P_{O2}^{(2)}$ values were set by mixing of gaseous O_2 and N_2 in proper ratios, $P_{O2}^{(1)} = 0.21$ atm. It was shown that the asymmetric potential value measured at ($P_{O2}^{(1)}$) = $P_{O2}^{(2)}$ =0.21 atm. in the temperature range 773-1073K [12,13] was less than 5 mV for all studied electrolytes.

Fig. 11 depicts E_{real} dependencies on the oxygen partial pressure with respect to the amendment due to the asymmetric potential; these dependencies were measured at different temperatures for the solid electrolytes of different compositions synthesized from the precursor powders with different average agglomerate sizes. Nernst equation plots are also depicted in Fig. 11. The difference between E_{Nerns} and E_{real} for the discussed solid electrolytes is shown in Fig. 12. Table 2 lists the results of t_{ion} estimates.

Analyzing the data presented in Table 2, one can conclude that the input of electron conductivity increases with the increase in the average agglom-

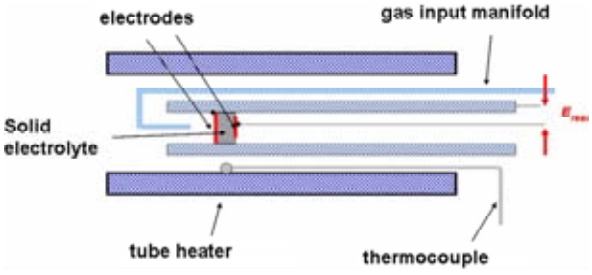

Fig. 10. The scheme of the oxygen sensor.

Table 2. Transport numbers of the oxygen ions (t_{ion}) estimated for the temperature range 870-1060K for the solid electrolytes studied.

Composition of solid electrolyte, mol.%	Average agglomerate size in the precursor, nm	t_{ion}
$0.08Y_2O_3$-$0.92ZrO_2$	40	0.98
	100-140	0.97
	200-250	0.81
$0.09Ce_2O_3$-$0.91ZrO_2$	100-150	0.93
$0.06Ce_2O_3$-$0.06Y_2O_3$-$0.88ZrO_2$	100-150	0.88

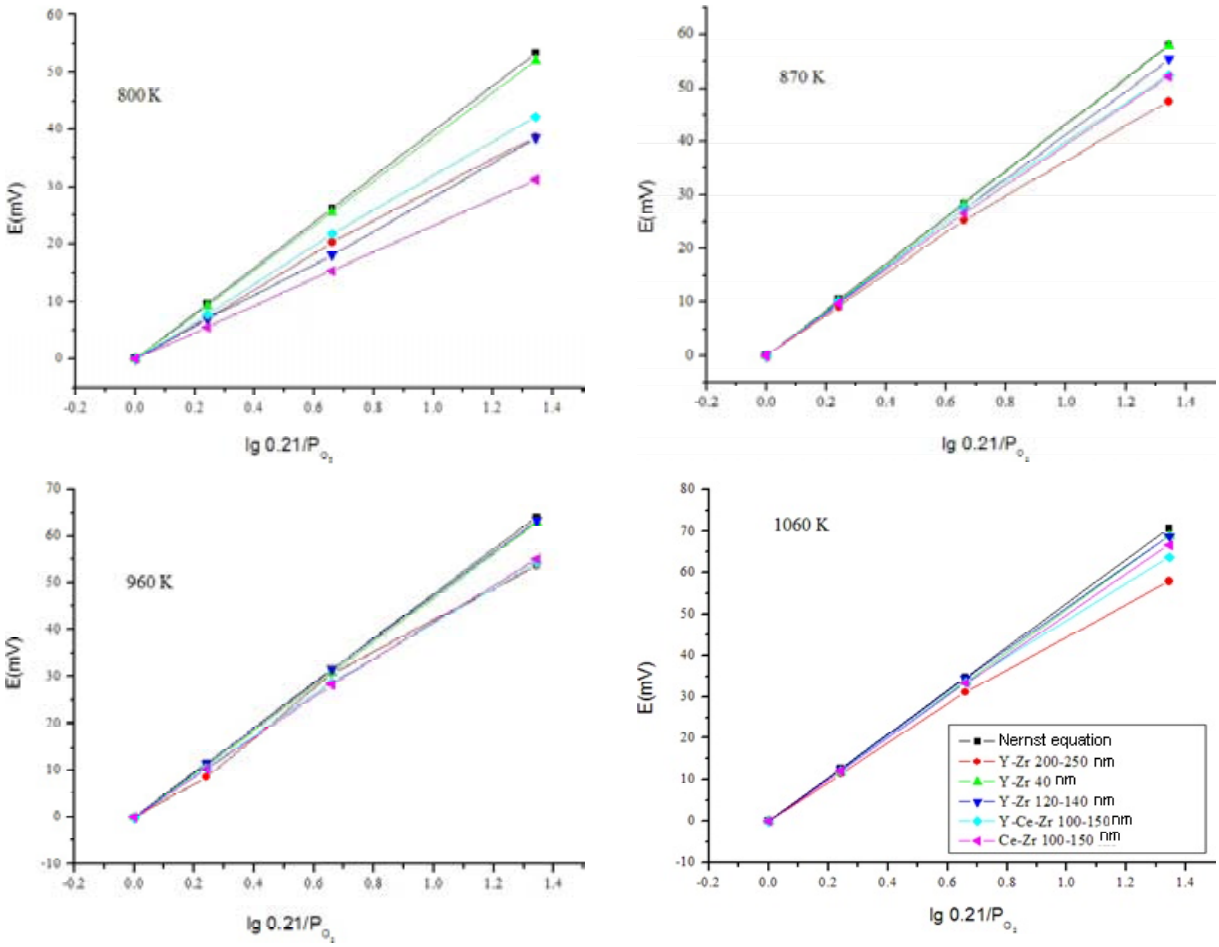

Fig. 11. EMF dependencies (*E*) of the oxygen sensors with solid electrolytes synthesized from the precursor powders with different average agglomerate size on the oxygen partial pressures.

erate size in the precursors. Lower t_{ion} values obtained for cerium-containing electrolytes are possibly due to the presence of multivalent cerium ions in these electrolytes. As follows from Fig. 11 and Table 2, sensors based on yttrium-zirconia solid electrolytes manufactured from the precursor powders with the average agglomerate size of 40 and 100-140 nm possess the best sensor properties at temperature decrease down to $T \approx 873$K.

Fig. 13 demonstrates the comparison of sensor properties of the sensors based on yttrium-zirconia solid electrolytes manufactured from the precursor powders with the average agglomerate size of 40 and 100-140 nm with the sensors produced by conventional solid-phase approach; the advantage of sensors synthesized from nanosized precursors is evident.

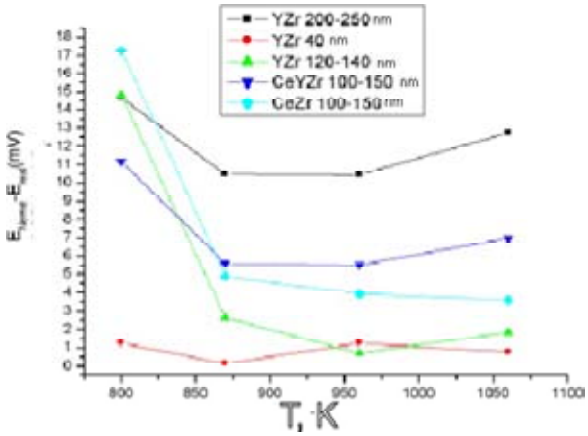

Fig. 12. Temperature dependencies of the difference between the theoretical and experimental values of the electromotive force (**E_{Nernst} - E_{real}**) at $P_{O2}^{(2)}$ = $9.5 \cdot 10^{-3}$ atm for the studied sensors with solid electrolytes synthesized from the precursor powders with different average agglomerate size.

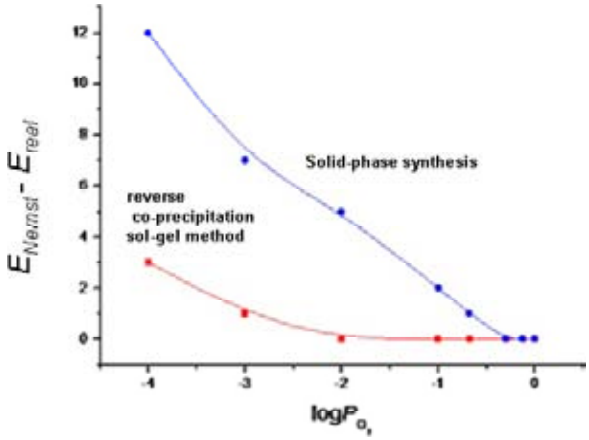

Fig. 13. The dependencies of the difference between theoretical and experimental electromotive force values (**E_{Nernst} - E_{real}**) for the sensors with solid electrolytes produced by different methods on oxygen partial pressure ($P_{O2}^{(2)}$) at 973K.

The response time for the sensors with solid electrolytes synthesized from nanosized precursor powders for the deviation of oxygen partial pressure ($P_{O2}^{(2)}$ = 0.01 atm., $P_{O2}^{(1)}$ = 0.21 atm.) was quite similar in the wide temperature range, at T ≥ 923K it is 1-2 sec. in all.

Thus, in can be stated that oxygen sensors based on $0.08Y_2O_3$-$0.92ZrO_2$ solid electrolytes synthesized from the precursors with the average agglomerate size 100-140 nm possess better exploitation characteristics than the sensors with the same composition produced by solid phase synthesis; in addition, the temperature range of their exploitation can be decreased by ≈200K. At the moment, oxygen sensors based on such solid electrolytes manufactured from nanosized precursor powders are produced by Smolensk State Production Union "Analitpribor" (Smolensk, Russia); these sensors are used by Russian and foreign companies working in the field of fuel and energy.

4. CONCLUSIONS

A number of solid electrolytes for oxygen sensors based on zirconia ceramics was produced from nanosized precursor powders synthesized by reverse co-precipitation sol-gel method. A complex study of the effect of the precursors average agglomerate size on the conductivity and sensor properties of the final ceramics was performed using PSD, DSC, XRD, BET, and ESCA techniques. It was shown that the increase in the precursor dispersity results in the increase in the conductivity and in the decrease of the exploitation temperature of the ceramics. The results obtained in the study form the base for the industrial production of the oxygen sensors used in the different field of modern technology.

ACKNOWLEDGEMENT

The work was supported by the Russian Ministry of Education and Science (Contracts 14.740.11.0353 and 8025).

REFERENCES

[1] V.B. Glushkova and E.K. Keller, In : C*hemistry and technology of silicate and refractory non-metal materials* (Nauka, Leningrad, 1989), p. 41, In Russian.

[2] G.A. Semenov and A.N. Belov, In: *Chemistry of silicates and oxides* (Nauka, Leningrad, 1982), p. 211, In Russian.

[3] P. Kofstad, *Nonstoichiometry, Diffusion, and Electrical Conductivity in Binary Metal Oxides* (R.E. Krieger Publishing Company, 1972).

[4] I.N. Vasserman, *Chemical precipittion from solutions* (Nauka, Leningrad, 1980), In Russian.

[5] N.A. Toropov, V.P. Barzakovski, I.A. Bondar' and Yu. P. Udalov, *Phase diagrams of silicate systems, Handbook, part 2* (Nauka, Leningrad, 1970), In Russian.

[6] Powder Diffraction File (PDF-2). Release 2007.

[7] Yu. D. Tretyakov and Yu. D. Metlin, In: n: *Chemistry of silicates and oxides* (Nauka, Leningrad, 1982), p. 225, In Russian.
[8] R.L. Muller, *Electric conductivity of glassy substances* (Nauka, Leningrad, 1968), in Russian.
[9] U. Brossmann, G. Knöner, H.-E. Schaefer and R. Würschum // *Rev. Adv. Mater. Sci.* **6** (2004) 7.
[10] T.I. Politova and J.T.S. Irvin // *Solid State Ionics* **168** (2004) 153.
[11] F. A Kroger, *The chemistry of imperfect crystals* (Interscience Publishers, 1964).
[12] V.S. Galkin, V.G. Konakov, A. V. Shorohov and E.N. Solovieva //
Rev. Adv. Mater. Sci **10** (2005) 3.
[13] V.G. Konakov and A. V. Shorohov, In: *High temperature chemistry of silicates and oxides* (Nauka, Saint Petersburg, 2002), p. 179.